iScience

CellPress
OPEN ACCESS

Article

# Direct visualization of floppy two-dimensional DNA origami using cryogenic electron microscopy

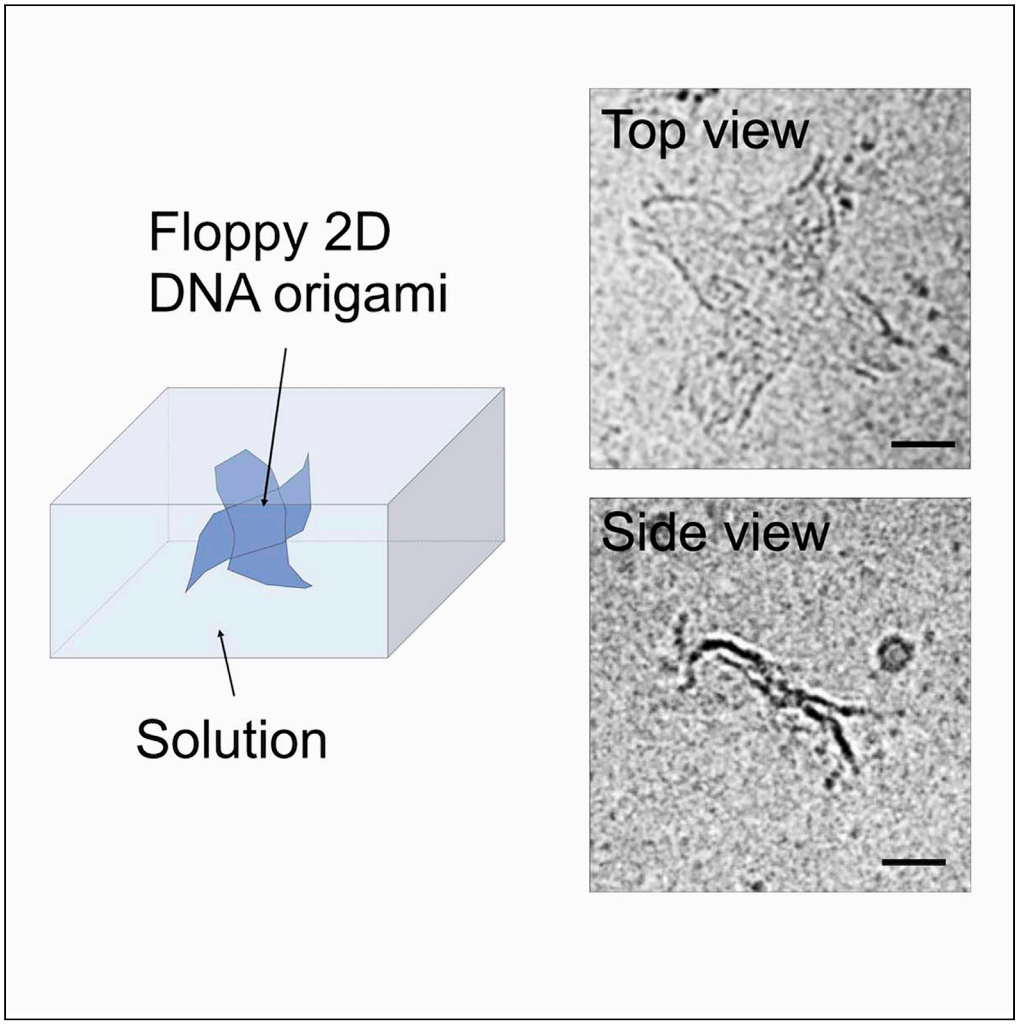


Heng Ni, Xiao Fan, Feng Zhou, ..., Nan Yao, Paul M. Chaikin, Yimo Han

nyao@princeton.edu (N.Y.)
chaikin@nyu.edu (P.M.C.)
yimo.han@rice.edu (Y.H.)

## Highlights

2D DNA origami is floppy in solution

Cryo-EM pictures unstained monolayer DNA origami with details

2D DNA origami cross-tiles have flexible arms and form clusters and stacks

Dimmer and trimmer complexes can fold in solution on design

Ni et al., iScience *25*, 104373
June 17, 2022 
https://doi.org/10.1016/j.isci.2022.104373

iScience

CellPress
OPEN ACCESS

Article

# Direct visualization of floppy two-dimensional DNA origami using cryogenic electron microscopy

Heng Ni,[1] Xiao Fan,[2] Feng Zhou,[1] Galio Guo,[3] Jae Young Lee,[4] Nadrian C. Seeman,[6] Do-Nyun Kim,[4] Nan Yao,[5,*] Paul M. Chaikin,[1,*] and Yimo Han[3,7,*]

## SUMMARY

**Two-dimensional (2D) DNA origami that is capable of self-assembling into complex 2D and 3D geometries pave the way for a bottom-up synthesis for various applications in nano/biotechnology. Here, we directly visualized the aqueous structure of 2D DNA origami cross-tiles and their assemblies using cryogenic electron microscopy. We uncovered flexible arms in cross-tile monomers and designated inter-tile folding. In addition, we observed the formation of clusters and stacks of DNA cross-tiles in solution, which could potentially affect the interaction and assembly of DNA origami. Finally, we quantitatively evaluated the flexibility of DNA origami in solution using finite element analysis. Our discovery has laid the foundation for investigating the dynamic structures of 2D DNA origami assemblies in solution, providing insights regarding the self-assembly and self-replication mechanisms of 2D DNA origami.**

## INTRODUCTION

Scaffolded DNA origami, the key development in DNA nanotechnology, can create arbitrarily shaped two-dimensional (2D) and three-dimensional (3D) DNA nanostructures (Andersen et al., 2009; Bai et al., 2012; Dietz et al., 2009; Gerling et al., 2015; Han et al., 2011; Iinuma et al., 2014; Ke et al., 2009a, 2009b; Marras et al., 2015; Zhang et al., 2018a). It combines a long single-stranded scaffold DNA with a pool of short-staple strands that fold it into a programmable nanostructure. By predesigning the monomeric DNA nanostructures and precisely tuning the hybridization of single-stranded sticky ends, the self-assembly of DNA origami could be specified to build gigadalton-scale structures (Iinuma et al., 2014; Liu et al., 2011; Zhang et al., 2018a), engendering applications such as metamaterial (Lee et al., 2012; Tian et al., 2020) and self-replication (He et al., 2017; Wang et al., 2011; Zhuo et al., 2019) devices. Specifically, 2D DNA origami usually has a highly confined thickness compared with their in-plane dimensions. They have been used as building blocks for 2D lattices both in solution (Liu et al., 2011) and on surfaces (Suzuki et al., 2015; Woo and Rothemund, 2014), as well as a functioning platform for the programmable assembly of hybrid and reconfigurable structures (Zhang et al., 2018b; Zion et al., 2017).

However, understanding the native shape of 2D DNA origami in solution still relies on theoretical predictions (Castro et al., 2011; Kim et al., 2012; Lee et al., 2021; Maffeo and Aksimentiev, 2020). We postulate they will be floppy in solution owing to their softness and flexibility, which may affect their intermolecular properties and interactions. Conventional imaging techniques, such as atomic force microscopy (AFM) and negatively stained transmission electron microscopy (TEM), have been widely used to investigate DNA origami (Douglas et al., 2009a; Han et al., 2011; Ke et al., 2012a, 2014; Liu et al., 2011; Rothemund, 2006; Wei et al., 2012; Woo and Rothemund, 2011; Yang et al., 2012; Zhou et al., 2021). However, these techniques require the deposition of 2D origami tiles onto a flat surface. As 2D origami tightly stitches to the flat surface owing to electrostatic interactions (Figures 1A and 1B), the genuine 3D structure of the aqueous 2D origami (Figure 1C) cannot be determined through this process. Thus, the use of a method that can directly visualize the 2D origami in solution is crucial for investigating the floppiness of 2D DNA origami.

Cryogenic electron microscopy (cryo-EM) directly satisfies these challenges. In this approach, samples are immobilized in solution via vitrification (Dubochet, 2012), the rapid freezing of water into amorphous ice to avoid crystallization and volume expansion, which guarantees that biomolecules are frozen in their original states in solution. For several decades, cryo-EM has been widely used to investigate the 3D structure of proteins (Kühlbrandt, 2014). Although several groups have adopted this technique to reveal static and

[1]Department of Physics, New York University, New York, NY 10003, USA

[2]Department of Molecular Biology, Princeton University, Princeton, NJ 08544, USA

[3]Department of Materials Science and NanoEngineering, Rice University, Houston, TX 77005, USA

[4]Department of Mechanical Engineering, Seoul National University, Seoul 08826, Republic of Korea

[5]PRISM Imaging and Analysis Center, Princeton University, Princeton, NJ 08544, USA

[6]Department of Chemistry, New York University, New York, NY 10003, USA

[7]Lead contact

*Correspondence: nyao@princeton.edu (N.Y.), chaikin@nyu.edu (P.M.C.), yimo.han@rice.edu (Y.H.)

https://doi.org/10.1016/j.isci.2022.104373

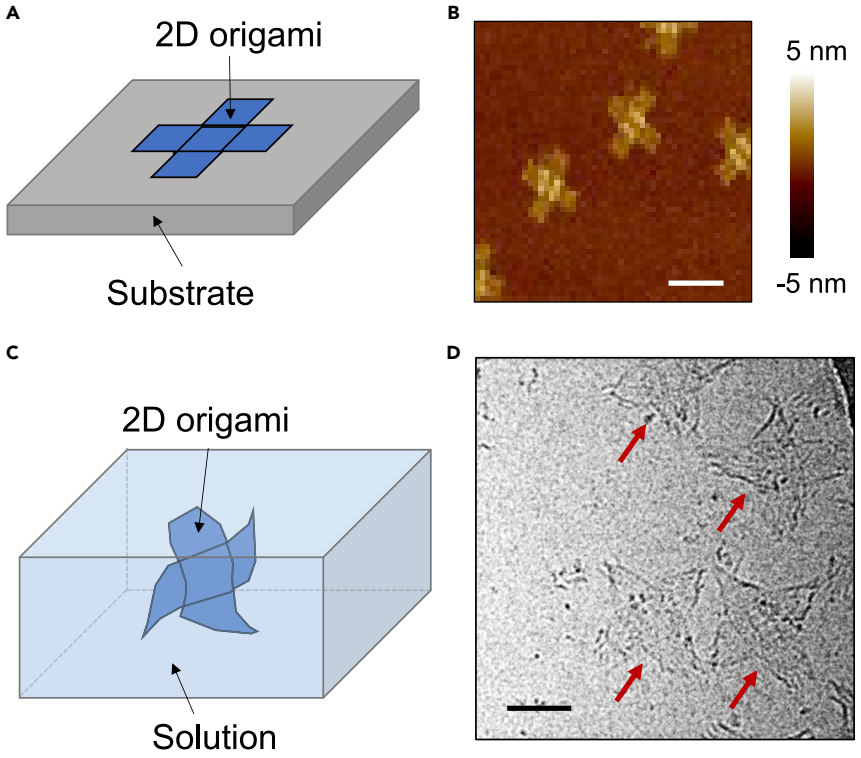


**Figure 1. Floppy 2D DNA origami cross-tiles in solution**

(A) Schematic of a 2D origami cross-tile deposited on a flat surface.

(B) AFM image of 2D origami cross-tiles on a mica surface.

(C) Schematic of a 2D origami cross-tile in solution (scale bar: 100 nm).

(D) Cryo-EM micrograph of a few 2D origami cross-tiles (pointed by red arrows) in vitrified ice, representing their native morphology in solution (scale bar: 50 nm).

dynamic structures of DNA origami (Bai et al., 2012; Ke et al., 2009a, 2012b; Lei et al., 2018; Liu et al., 2016), they utilized single particle analysis to study the rigid 3D DNA origami structure by averaging images of many particles. However, single particle analysis does not apply to floppy 2D DNA origami owing to their distinct shapes. In addition, monolayer DNA origami is much harder to visualize than 3D DNA origami because of the low signal. Here, we demonstrate the direct visualization of the genuine morphology of 2D origami in solution (Figure 1D) by optimizing imaging conditions. We utilized the most advanced 300 kV cryo-EM equipped with an energy filter and a direct electron detector. We observed as-synthesized and non-stained DNA cross-tiles with flexible arms and further investigated their dimer and trimer assemblies in vitrified ice.

## RESULTS

### Synthesis of 2D DNA cross-tile

The 2D DNA origami design used in this investigation was previously reported by Liu et al., in 2011 (Liu et al., 2011). The double-layer DNA origami cross-tile structure of this design was chosen for the propensity of each origami cross-tile to potentially act as building blocks for larger modular 2D or 3D configurations, whose properties and final anatomy can be customized through modifications in the sticky ends of individual flakes. In our study, we first used caDNAno (Douglas et al., 2009b), a computer-aided design software for DNA origami, to generate the cross-tile shape following the original design by Liu et al. Next, a long single-stranded DNA (ssDNA) sourced from the M13 bacteriophage (M13MP18), was utilized as the scaffold DNA (Figure 2A) across the entire 2D DNA cross-tile. An additional ~250 short ssDNA staple strands (Figure 2B) were utilized to establish the cross-tile shape of the 2D DNA origami by bridging regions of the scaffold ssDNA. The scaffold DNA was combined with these staple strands by heat-annealing the mixture, allowing the DNA origami cross-tiles to self-assemble. After synthesis, we purified the DNA cross tiles by

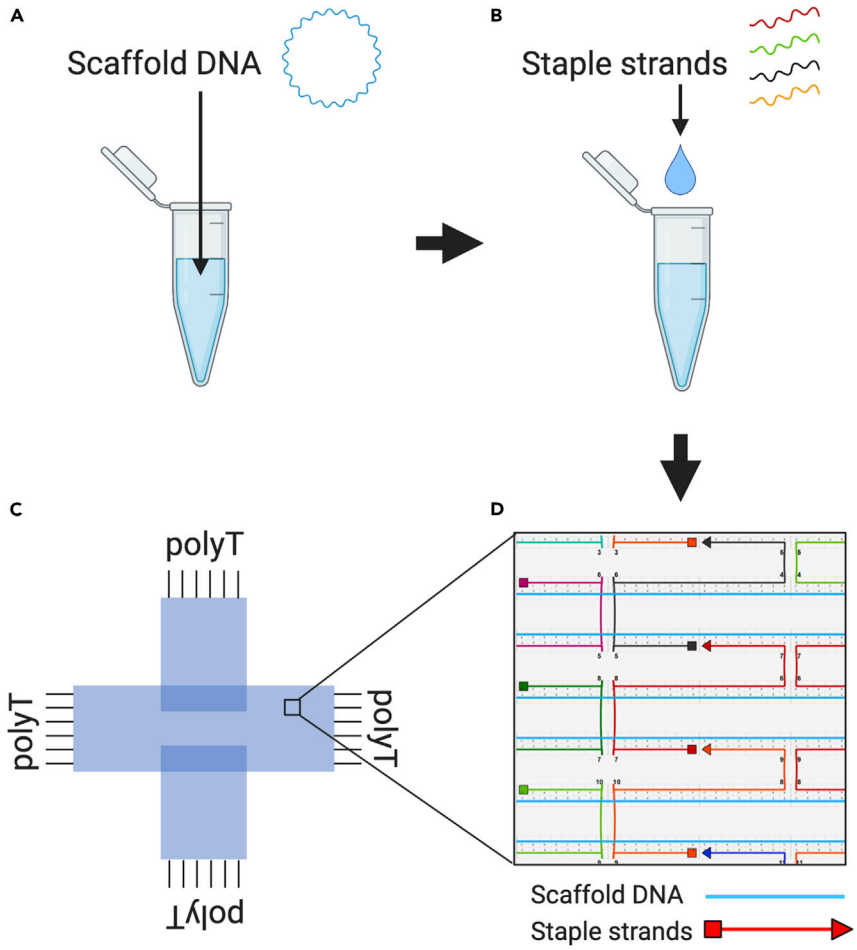


**Figure 2. Synthesis of 2D DNA cross-tiles**

(A) Schematic of scaffold DNA in buffer solution.

(B) Adding staple strands into the scaffold DNA solution.

(C) Final product, where the scaffold DNA folds into a designated shape assisted by the staple strands.

(D) Zoomed-in illustration of the DNA cross-tile, where the blue ssDNA is part of the scaffold DNA and ssDNA of other colors are individual staple strands.

filtering the solution to remove excess staple DNA strands. More details of the synthesis can be found in STAR Methods. The ultimate result was a DNA cross-tile with 4 monolayer arms and a double-layered center that resembled an equality symbol (Figure 2C), which was confirmed by the air-mode AFM (Figures 1B and S1). The monolayer region adopted a chicken-wire-like structure (Figure 2D) owing to the arrangements of scaffold and staple DNA strands. To prevent blunt-end stacking, the DNA cross-tiles were protected by poly-T sticky ends at their extruding edges on all four arms, which were implemented into the design through the staple strands (Figure 2C).

## Imaging 2D DNA cross-tiles in solution via cryo-EM

After producing the 2D DNA cross-tiles, they were directly deposited onto the carbon side of freshly plasma-treated Quantifoil cryo-EM grids for cryo-sample preparation (More details in STAR Methods). We allowed the sample to sit on the cryo-EM grid for 30 s in a humidity-controlled chamber and then performed a short blotting process using two filter papers to reduce the sample to a thin layer of solution. Then followed by a rapid plunge process, the sample was fast frozen in liquid ethane for vitrification.

Under the cryo-EM imaging, the DNA origami cross-tiles appeared to exist as individual flakes, diffuse clusters, and dense stacks (Figure 3A). Individual flakes demonstrated uneven morphology (Figures 1D,3B, and

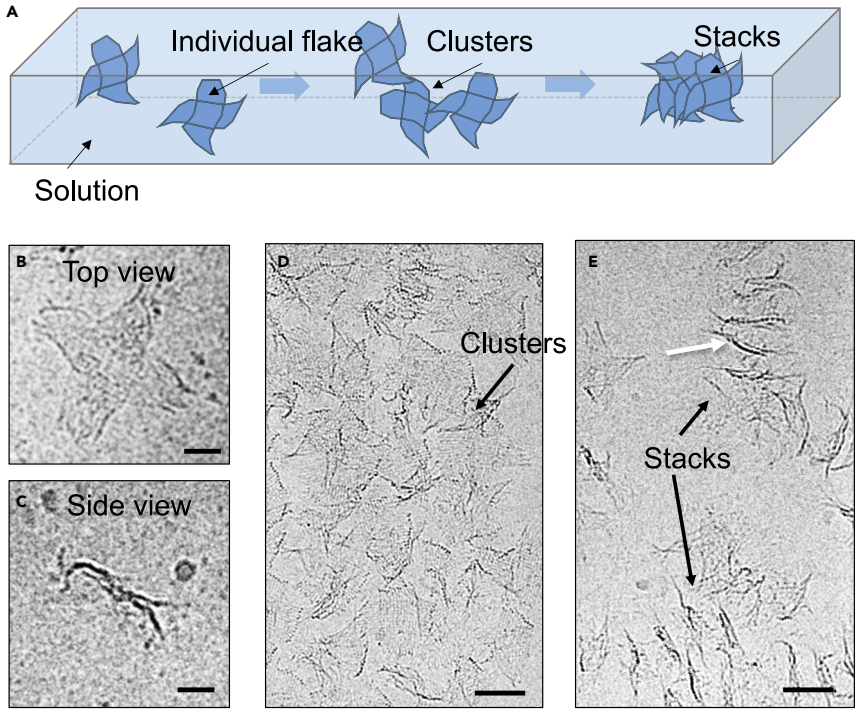


**Figure 3. Cryo-EM investigation of 2D DNA origami's morphology and interactions**

(A) Schematic of DNA cross-tiles and their interactions in solution.

(B and C) Cryo-EM micrograph of individual DNA cross-tile monomers. Individual flakes show both top view (B) and side view (C). Scale bars for (B) and (C): 20 nm.

(D) Cryo-EM micrograph of DNA clusters. Figure S5 shows a comparison of top and side views with simulation results.

(E) Cryo-EM micrograph showing stacks of DNA cross-tiles formed in solution. White arrow indicates dark lines that represent a side view. Scale bars for (D) and (E): 50 nm.

3C). The center squares appear more rigid owing to the double layer equal sign, while the four arms of the cross-tile appear to possess additional flexibility. A gallery of the monomers shows that each of them adopts a distinct shape, especially for the flexible arms (Figure S2). An electron tomogram containing a 3D structure of two monomers in solution (Figure S3, and Movies S1, S2) also confirmed the flexible arms. This was attributed to the lower stiffness of the DNA monolayer region compared to the bilayer region at the equality symbol in the center square. As the four arms exhibited greater flexibility with their edges exposed to the environment, we expect that this morphology of monomer cross-tiles in solution may encourage intermolecular edge-to-edge contacts between different flakes to form larger, multiple cross-tile assemblies upon design. However, owing to the limited dose put on the sample, we were not able to unveil high-resolution 3D structure. The dose evaluation of the DNA origami by cryo-EM is discussed in Figure S4.

In addition, we observed that individual flakes tended to aggregate and form clusters (Figures 3D and S5). In AFM, neither air nor liquid modes were able to show the native morphology of the clusters (Figure S6), as electrostatic forces collapsed the clusters onto the substrate, leaving their 3D structures unknown. In contrast, cryo-EM records the projection images of the cross-tile clusters in solution, allowing us to observe the natural orientation and morphology of cross-tiles in the cluster. As shown in Figure 3D, the cryo-EM micrograph reveals that DNA cross-tiles randomly adhere and form multi-flake clusters, where the interaction introduces additional twists in DNA cross-tiles. In our study, we also observed stacks, where individual cross-tiles in the stacks aggregated along the entirety of their faces (Figure 3E), which might be the consequence of a continuous clustering and aggregation of cross-tiles in solution. The image contrast of the 2D origami under cryo-EM also permitted additional insight into the morphology of the stacks, which do not show completely random interactions. The dark lines (white arrows in Figure 3E) in the cryo-EM micrograph are from center squares of the DNA cross-tiles and exist in an orientation parallel to the electron beam, consistent with a side view of the monomer (Figures 3C and S7). This allowed us to conclude that the center

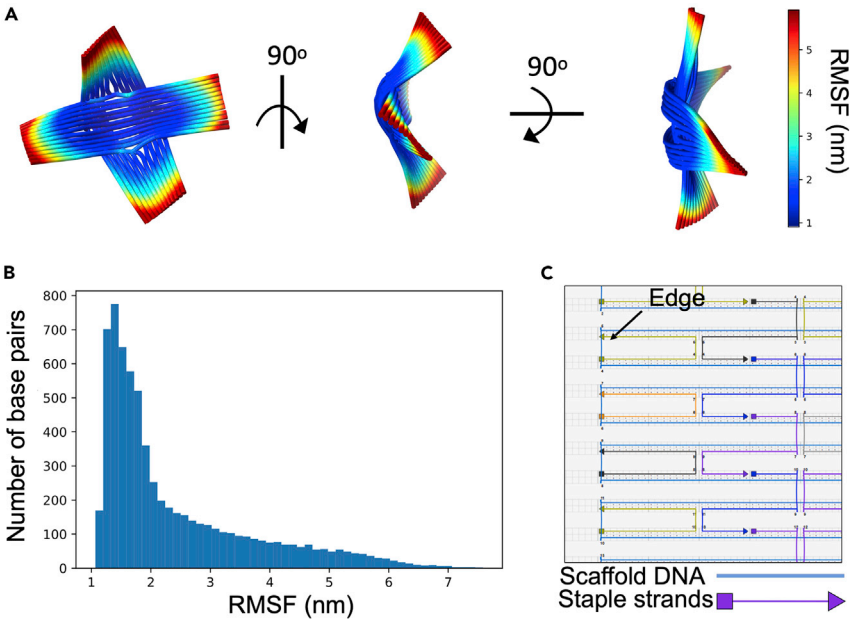


**Figure 4. Finite element analysis of 2D cross-tiles via CanDo**

(A) Morphology of DNA cross-tile from CanDo. Color mapping refers to root mean square fluctuations (RMSFs), which indicate the flexibility of the DNA cross-tiles.

(B) Histogram of the RMSFs in a single DNA cross-tile.

(C) Illustration of the cross-tile edges, where there is maximum flexibility.

squares of cross-tiles possessed a coherent orientation in the stacked superstructure. Additional investigation of the positively stained sample confirmed the existence of clusters and stacks with a clearer contrast (Figure S8). Although it remains unclear precisely how the short-range attractive forces between individual strands inform the observed interactions between cross-tiles, our observations of the monomeric 2D DNA origami in solution have imparted insight into the aqueous behavior and morphology of 2D DNA origami, which is crucial for understanding the steric requirement for their self-assembly behavior for future applications of this technology.

## Shape and flexibility of 2D DNA cross-tiles using finite element analysis

In order to confirm our observations made through cryo-EM and further quantitatively elucidate the flexibility of the 2D DNA flakes in solution, we used CanDo (Castro et al., 2011; Kim et al., 2012) to perform finite element analysis (More details in STAR Methods). By treating dsDNA as elastic rods, energy minimized conformations of DNA origami structures can be predicted from the initial caDNAno design. The predictions directly visualized the aqueous geometry of the DNA origami in 3D (Figure 4A) and quantified the regional flexibilities of the cross-tile through root-mean square fluctuations (RMSFs) (Figure 4B), which are widely used to describe deformed 3D structures in thermal equilibrium (McQuarrie, 1975).

From the calculation, we identified the twisted morphology of the origami cross-tile (Figure 4A). The deviations from a purely flat, undistorted structure appear in both half tiles and are caused by the supercoiling in dsDNA strands within the origami. In the square design, 2D origami uses ~10.7 base pairs for every turn in the crossover strands between helices, while natural B-DNA has around 10.5 base pairs per turn. The 0.2 base pair per turn difference leads to a dramatic change in geometry for DNA origami cross-tiles owing to the large number of base pairs included in the sample (~288 bps in one helix in our design), causing the observed twisting deformation (Baker et al., 2018). The linking staple strands that connect the two tiles assert further strain to the 2D origami flake, leading to non-symmetric distortion between the two tiles. Although this bend and twist in 2D cross-tiles is well understood and can be removed via proper design, we did not clearly observe the distortion in cryo-EM images owing to the diverse shapes found in solution. We believe the shape of 2D DNA origami is dominated by its flexibility in solution.

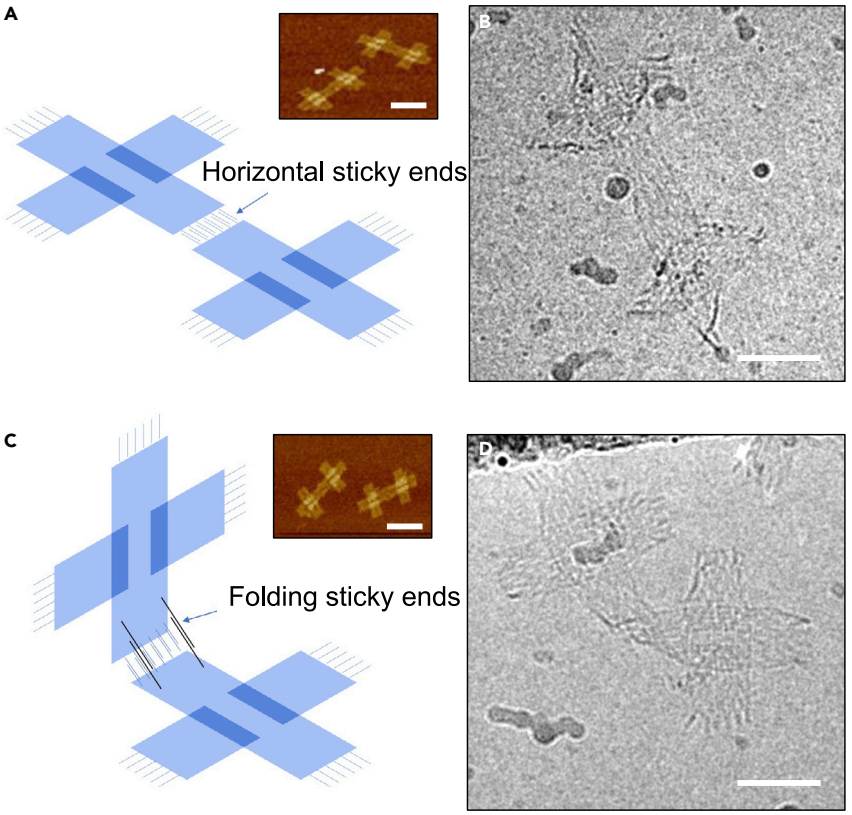


**Figure 5. Self-assembled 2D DNA cross-tile dimers**

(A) Design of a flat 2D DNA origami dimer, which may form via horizontal sticky ends to crosslink flakes. Inset: AFM image of synthesized flat dimers (scale bar: 100 nm).

(B) Cryo-EM micrograph of synthesized flat DNA dimers (scale bar: 50 nm).

(C) Design of a folded 2D DNA origami dimer by adding additional folding stands. Inset: AFM image of synthesized folded dimers (scale bar: 100 nm).

(D) Cryo-EM micrograph of folded dimers, including a fold between two monomers (scale bar: 50 nm).

We further characterized the flexibility of the cross-tile using CanDo through RMSF, illustrated via color mapping on the predicted energy-minimized conformation in Figure 4A. Lower and higher RMSF corresponded to smaller and greater flexibility, respectively. In our work, lower flexibility was expected in the center square of the cross-tile as it is a region where two sheets of DNA origami overlap. In contrast, the four arms possessed greater flexibility because they were single-layered. We also performed a statistical study on the distribution of RMSF on the predicted cross-tile structure (Figure 4B). In the histogram, the number of base pairs peak at around 1.5 nm. This corresponds to the center square of the cross-tile and adjoining nucleotides on the four outer arms (blue region in Figure 4A), which comprises a majority of the total nucleotides in the design. The cross-tile increases in flexibility as the outer edges are approached, corresponding to a continuous tail in the histogram, and attains maximum RMSF at the terminus of each of the four extruding arms. These maxima may be attributed to the loose staple strands designed for the edges of DNA cross-tiles (Figure 4C). In contrast to conventional designs where neighboring helices are linked by one crossover staple strand for every 32 nucleotides, we have adopted 16 leftover nucleotides with no securing crossover staple strand. Therefore, the most flexible regions in the entire structure are located at the ends of helices. Additional simulation results (Figure S9 and supplementary file 2) from SNUPI (Lee et al., 2021) provide consistent results with the CanDo method. We postulate this may make them more active to bind to each other and assemble into large complexes, but additional experiments are required to back it up.

## Self-assembled dimers and trimers in solution

Before investigating the complete scope of possibilities for large, highly ordered, modular DNA origami superstructures, the adjustments in the properties and morphology of 2D DNA origami monomers once

they are coupled together must be understood. To this end, we combined two monomeric flakes into a dimer design with six 11-nucleotide horizontal sticky ends (Figures 5A, S10, and Table S1). We subsequently investigated the design under AFM and cryo-EM (Figure 5B). We designed two types of dimers, with and without folding strands on the adjacent planes. The folding strands are strut-like double-stranded DNA on the adjacent planes that can hybridize and help the dimer to fold into a 3D structure (Figure 5C). The length of the DNA strut was determined by the location of the strut on the origami plate, the linker length, and the angle between the two origami plates. The AFM images (insets of Figures 5A, 5C, and S11) show that mica substrates disrupt the 3D structure and flatten most of the dimers owing to the strong electrostatic interaction between the two. In contrast, cryo-EM micrographs uncover a folding trend for most folded dimers (Figures 5B, 5D). However, owing to the flexibility of native dimers, we observed an over-fold in the cryo-sample, possibly introduced by the ice thickness confinement. We did not observe a 90-degree folding as shown in the schematic (Figure 5C). In addition, the dimers also demonstrate floppy free arms in solution (Figures 5B, 5D, and S12), which do not appear in AFM images. The connected arms become less flexible owing to the hybridization of horizontal sticky ends.

We also designed and synthesized a trimer complex with a folding strand (Figure S13). However, as trimers cannot be concentrated to the ideal concentration for cryo-EM sample preparation, none of the trimers was observed during sample searching. Therefore, we utilize a graphene cryo-EM grid (Han et al., 2019) to increase the adsorption of trimers (More details in STAR Methods). However, graphene surfaces to some extent disrupt the 3D trimer structure, making them flat in cryo-EM micrographs (Figure S14). Therefore, we utilized uranyl acetate to strain the DNA trimers to increase their strength. In the cryo-EM imaging, we observed the folding in the trimer, which was intentionally designed and realized by the folding strands (Figure S15). In order to better view the folds, we tilted our sample from $-20^{\circ}$ to $20^{\circ}$ (Figure S16). Although electron beam damage on the sample was observed during the cryo-micrograph acquisition, we were able to distinguish different projection images and confirm the bend we observed is a 3D fold in the DNA origami trimer.

Owing to the challenging preparation of trimer samples, the observed trimers were limited. Accordingly, we utilized an SNUPI finite element analysis to predict the natural shape of the trimer. The predicted structure (Figures S17 and S18) shows a similar $90^{\circ}$ folding intentionally introduced by the designed folding strand, supporting the observation in cryo-EM. Additionally, the trimer exhibited remarkably higher RMSF than the monomer as the comprising monomers could fluctuate around sticky ends that served as flexible joints between monomers.

## DISCUSSION

We have used cryo-EM to directly observe the morphology of 2D DNA origami in solution. The results show flexible arms in 2D DNA cross-tiles, leading to a floppy shape rather than a rigid structure with inner torsion. The experiments also reveal the presence of clustered and stacked superstructures. In addition, our results also present the folding of dimers and trimers controlled by the design of folding sticky ends. Finally, finite element analysis corroborates the observations made under cryo-EM and provides quantitative insights into the flexibility of both monomers and dimer and trimer assemblies. The research paves the way for a better understanding of floppiness of 2D DNA origami in solution.

### Limitations of study

Although we observed the floppiness of 2D DNA origami, we have not shown a high-resolution 3D structure from cryo-EM owing to the low signal and electron dose limit. Our 3D reconstruction from a cross-tile monomer (shown in Figure S3 and Movies S1 and S2) provides limited information to determine the 3D structure. Future technique advancements that can provide high-resolution 3D cryo-EM structure of individual 2D DNA origami will lead to a better understanding of the flexibility and dynamics of 2D DNA origami.

## STAR★METHODS

Detailed methods are provided in the online version of this paper and include the following:

- KEY RESOURCES TABLE
- RESOURCE AVAILABILITY
  - Lead contact
  - Materials availability
  - Data and code availability

## SUPPLEMENTAL INFORMATION

Supplemental information can be found online at https://doi.org/10.1016/j.isci.2022.104373.

## ACKNOWLEDGMENTS

G.G. and Y.H. are supported by a Research grant from Welch Foundation (Grant #: C-2065-20210327). F.Z. acknowledges DOE DE-SC0007991 for DNA and origami synthesis. H.N. acknowledges the Center for Bio-Inspired Energy Sciences, an Energy Frontier Research Center funded by the DOE, Office of Sciences, Basic Energy Sciences, under award no. DE-SC0000989 for the simulation of the origami structure. J.Y. L. and D.-N. K. are supported by the National Convergence Research of Scientific Challenges (NRF-2020M3F7A1094299) and the Basic Research Program (NRF-2019R1A2C4069541) through the National Research Foundation of Korea (NRF) funded by the Ministry of Science and ICT. The authors acknowledge the use of Princeton's Imaging and Analysis Center, which is partially supported by the Princeton Center for Complex Materials, a National Science Foundation (NSF)-MRSEC program (DMR-2011750). This work also made use of the Electron Microscopy Center at Rice University. We thank Mark Bathe for help on the CanDo simulation (Castro et al., 2011; Kim et al., 2012). We thank Ruojie Sha and Chuqiao Shi for their helpful discussion.

## AUTHOR CONTRIBUTIONS

Conceptualization, Y.H. and F.Z.; Methodology, H.N., X.F., F.Z., G.G., J.Y.L., and D.-N.K.; Investigation, Y.H., H.N., X.F., and F.Z.; Writing – Original Draft, Y.H., H.N., F.Z., and G.G.; Review & Editing, Y.H., H.N., X.F., and F.Z.; Funding Acquisition, Y.H., N.Y., and P.C.; Resources, N.Y.; Supervision, Y.H., P.C., and N.Y.

## DECLARATION OF INTERESTS

The authors present no competing interests.

Received: August 4, 2021
Revised: April 19, 2022
Accepted: May 4, 2022
Published: June 17, 2022

## REFERENCES

Andersen, E.S., Dong, M., Nielsen, M.M., Jahn, K., Subramani, R., Mamdouh, W., Golas, M.M., Sander, B., Stark, H., Oliveira, C.L.P., et al. (2009). Self-assembly of a nanoscale DNA box with a controllable lid. Nature *459*, 73–76. https://doi.org/10.1038/nature07971.

Bai, X.C., Martin, T.G., Scheres, S.H.W., and Dietz, H. (2012). Cryo-EM structure of a 3D DNA-origami object. Proc. Natl. Acad. Sci. U S A *109*, 20012–20017. https://doi.org/10.1073/pnas.1215713109.

Baker, M.A.B., Tuckwell, A.J., Berengut, J.F., Bath, J., Benn, F., Duff, A.P., Whitten, A.E., Dunn, K.E., Hynson, R.M., Turberfield, A.J., and Lee, L.K. (2018). Dimensions and global twist of single-layer DNA origami measured by small-angle X-ray scattering. ACS Nano *12*, 5791–5799. https://doi.org/10.1021/acsnano.8b01669.

Castro, C.E., Kilchherr, F., Kim, D.-N., Shiao, E.L., Wauer, T., Wortmann, P., Bathe, M., and Dietz, H. (2011). A primer to scaffolded DNA origami. Nat. Methods. *8*, 221–229. https://doi.org/10.1038/nmeth.1570.

Dietz, H., Douglas, S.M., and Shih, W.M. (2009). Folding DNA into twisted and curved nanoscale shapes. Science *325*, 725–730. https://doi.org/10.1126/science.1174251.

Douglas, S.M., Dietz, H., Liedl, T., Högberg, B., Graf, F., and Shih, W.M. (2009a). Self-assembly of DNA into nanoscale three-dimensional shapes. Nature *459*, 414–418. https://doi.org/10.1038/nature08016.

Douglas, S.M., Marblestone, A.H., Teerapittayanon, S., Vazquez, A., Church, G.M., and Shih, W.M. (2009b). Rapid prototyping of 3D DNA-origami shapes with caDNAno. Nucleic Acids Res. *37*, 5001–5006. https://doi.org/10.1093/nar/gkp436.

Dubochet, J. (2012). CryoEM—the first thirty years. J. Microsc. *245*, 221–224. https://doi.org/10.1111/j.1365-2818.2011.03569.x.

Gerling, T., Wagenbauer, K.F., Neuner, A.M., and Dietz, H. (2015). Dynamic DNA devices and assemblies formed by shape-complementary, non–base pairing 3D components. Science *347*, 1446–1452. https://doi.org/10.1126/science.aaa5372.

Han, D., Pal, S., Nangreave, J., Deng, Z., Liu, Y., and Yan, H. (2011). DNA origami with complex curvatures in three-dimensional space. Science *332*, 342–346. https://doi.org/10.1126/science.1202998.

Han, Y., Fan, X., Wang, H., Zhao, F., Tully, C.G., Kong, J., Yao, N., and Yan, N. (2019). High-yield

monolayer graphene grids for near-atomic resolution cryoelectron microscopy. Proc. Natl. Acad. Sci. U S A *117*, 1009–1014. https://doi.org/10.1073/pnas.1919114117.

He, X., Sha, R., Zhuo, R., Mi, Y., Chaikin, P.M., and Seeman, N.C. (2017). Exponential growth and selection in self-replicating materials from DNA origami rafts. Nat. Mater. *16*, 993–997. https://doi.org/10.1038/nmat4986.

Iinuma, R., Ke, Y., Jungmann, R., Schlichthaerle, T., Woehrstein, J.B., and Yin, P. (2014). Polyhedra self-assembled from DNA tripods and characterized with 3D DNA-PAINT. Science *344*, 65–69. https://doi.org/10.1126/science.1250944.

Ke, Y., Douglas, S.M., Liu, M., Sharma, J., Cheng, A., Leung, A., Liu, Y., Shih, W.M., and Yan, H. (2009a). Multilayer DNA origami packed on a square lattice. J. Am. Chem. Soc. *131*, 15903–15908. https://doi.org/10.1021/ja906381y.

Ke, Y., Sharma, J., Liu, M., Jahn, K., Liu, Y., and Yan, H. (2009b). Scaffolded DNA origami of a DNA tetrahedron molecular container. Nano Lett. *9*, 2445–2447. https://doi.org/10.1021/nl901165f.

Ke, Y., Ong, L.L., Shih, W.M., and Yin, P. (2012a). Three-dimensional structures self-assembled from DNA bricks. Science *338*, 1177–1183. https://doi.org/10.1126/science.1227268.

Ke, Y., Voigt, N.V., Gothelf, K.V., and Shih, W.M. (2012b). Multilayer DNA origami packed on hexagonal and hybrid lattices. J. Am. Chem. Soc. *134*, 1770–1774. https://doi.org/10.1021/ja209719k.

Ke, Y., Ong, L.L., Sun, W., Song, J., Dong, M., Shih, W.M., and Yin, P. (2014). DNA brick crystals with prescribed depths. Nat. Chem. *6*, 994–1002. https://doi.org/10.1038/nchem.2083.

Kim, D.-N., Kilchherr, F., Dietz, H., and Bathe, M. (2012). Quantitative prediction of 3D solution shape and flexibility of nucleic acid nanostructures. Nucleic Acids Res. *40*, 2862–2868. https://doi.org/10.1093/nar/gkr1173.

Kremer, J.R., Mastronarde, D.N., and McIntosh, J.R. (1996). Computer Visualization of Three-Dimensional Image Data Using IMOD. J Struct Biol *116*, 71–76. https://doi.org/10.1006/jsbi.1996.0013.

Kühlbrandt, W. (2014). Biochemistry. The resolution revolution. Science *343*, 1443–1444. https://doi.org/10.1126/science.1251652.

Lee, J.B., Peng, S., Yang, D., Roh, Y.H., Funabashi, H., Park, N., Rice, E.J., Chen, L., Long, R., Wu, M., and Luo, D. (2012). A mechanical metamaterial made from a DNA hydrogel. Nat. Nanotechnol. *7*, 816–820. https://doi.org/10.1038/nnano.2012.211.

Lee, J.Y., Lee, J.G., Yun, G., Lee, C., Kim, Y.-J., Kim, K.S., Kim, T.H., and Kim, D.-N. (2021). Rapid computational analysis of DNA origami assemblies at near-atomic resolution. ACS Nano *15*, 1002–1015. https://doi.org/10.1021/acsnano.0c07717.

Lei, D., Marras, A.E., Liu, J., Huang, C.-M., Zhou, L., Castro, C.E., Su, H.-J., and Ren, G. (2018). Three-dimensional structural dynamics of DNA origami Bennett linkages using individual-particle electron tomography. Nat. Commun. *9*, 592. https://doi.org/10.1038/s41467-018-03018-0.

Liu, W., Zhong, H., Wang, R., and Seeman, N.C. (2011). Crystalline twodimensional DNAorigami arrays. Angew. Chem. Int. Ed. *50*, 264–267. https://doi.org/10.1002/anie.201005911.

Liu, W., Tagawa, M., Xin, H.L., Wang, T., Emamy, H., Li, H., Yager, K.G., Starr, F.W., Tkachenko, A.V., and Gang, O. (2016). Diamond family of nanoparticle superlattices. Science *351*, 582–586. https://doi.org/10.1126/science.aad2080.

Maffeo, C., and Aksimentiev, A. (2020). MrDNA: a multi-resolution model for predicting the structure and dynamics of DNA systems. Nucleic Acids Res. *48*, 5135–5146. https://doi.org/10.1093/nar/gkaa200.

Marras, A.E., Zhou, L., Su, H.-J., and Castro, C.E. (2015). Programmable motion of DNA origami mechanisms. Proc. Natl. Acad. Sci. U S A *112*, 713–718. https://doi.org/10.1073/pnas.1408869112.

McQuarrie, D.A. (1975). Statistical Mechanics (Harper & Row).

Rothemund, P.W.K. (2006). Folding DNA to create nanoscale shapes and patterns. Nature *440*, 297–302. https://doi.org/10.1038/nature04586.

Scheres, S.H.W. (2012). A Bayesian View on Cryo-EM Structure Determination. Journal of Molecular Biology *415*, 406–418. https://doi.org/10.1016/j.jmb.2011.11.010.

Suzuki, Y., Endo, M., and Sugiyama, H. (2015). Lipid-bilayer-assisted two-dimensional self-assembly of DNA origami nanostructures. Nat. Commun. *6*, 8052. https://doi.org/10.1038/ncomms9052.

Tang, G., Peng, L., Baldwin, P.R., Mann, D.S., Jiang, W., Rees, I., and Ludtke, S.J. (2007). EMAN2: An extensible image processing suite for electron microscopy. Journal of Structural Biology *157*, 38–46. https://doi.org/10.1016/j.jsb.2006.05.009.

Tian, Y., Lhermitte, J.R., Bai, L., Vo, T., Xin, H.L., Li, H., Li, R., Fukuto, M., Yager, K.G., Kahn, J.S., et al. (2020). Ordered three-dimensional nanomaterials using DNA-prescribed and valence-controlled material voxels. Nat. Mater. *19*, 789–796. https://doi.org/10.1038/s41563-019-0550-x.

Wang, T., Sha, R., Dreyfus, R., Leunissen, M.E., Maass, C., Pine, D.J., Chaikin, P.M., and Seeman, N.C. (2011). Self-replication of information-bearing nanoscale patterns. Nature *478*, 225–228. https://doi.org/10.1038/nature10500.

Wei, B., Dai, M., and Yin, P. (2012). Complex shapes self-assembled from single-stranded DNA tiles. Nature *485*, 623–626. https://doi.org/10.1038/nature11075.

Woo, S., and Rothemund, P.W.K. (2014). Self-assembly of two-dimensional DNA origami lattices using cation-controlled surface diffusion. Nat. Commun. *5*, 4889. https://doi.org/10.1038/ncomms5889.

Woo, S., and Rothemund, P.W.K. (2011). Programmable molecular recognition based on the geometry of DNA nanostructures. Nat. Chem. *3*, 620–627. https://doi.org/10.1038/nchem.1070.

Yang, Y., Han, D., Nangreave, J., Liu, Y., and Yan, H. (2012). DNA origami with double-stranded DNA as a unified scaffold. ACS Nano *6*, 8209–8215. https://doi.org/10.1021/nn302896c.

Zhang, T., Hartl, C., Frank, K., Heuer-Jungemann, A., Fischer, S., Nickels, P.C., Nickel, B., and Liedl, T. (2018a). 3D DNA origami crystals. Adv. Mater. *30*, 1800273. https://doi.org/10.1002/adma.201800273.

Zhang, Y., He, X., Zhuo, R., Sha, R., Brujic, J., Seeman, N.C., and Chaikin, P.M. (2018b). Multivalent, multiflavored droplets by design. Proc. Natl. Acad. Sci. U S A *115*, 9086–9091. https://doi.org/10.1073/pnas.1718511115.

Zhuo, R., Zhou, F., He, X., Sha, R., Seeman, N.C., and Chaikin, P.M. (2019). Litters of self-replicating origami cross-tiles. Proc. Natl. Acad. Sci. U S A *116*, 1952–1957. https://doi.org/10.1073/pnas.1812793116.

Zhou, F., Sha, R., Ni, H., Seeman, N., and Chaikin, P. (2021). Mutations in artificial self-replicating tiles: a step toward Darwinian evolution. Proc. Natl. Acad. Sci. U S A *118*, e2111193118. https://doi.org/10.1073/pnas.2111193118.

Zion, M.Y.B., He, X., Maass, C.C., Sha, R., Seeman, N.C., and Chaikin, P.M. (2017). Self-assembled three-dimensional chiral colloidal architecture. Science *358*, 633–636. https://doi.org/10.1126/science.aan5404.

# STAR★METHODS

## KEY RESOURCES TABLE

| REAGENT or RESOURCE | SOURCE | IDENTIFIER |
|---|---|---|
| Oligonucleotides | | |
| Staple strands DNA | Integrated DNA Technologies | Custom DNA oligos |
| Recombinant DNA | | |
| M13mp18 single stranded phage DNA | Bayou Biolabs | Cat# P-107 |
| Software and algorithms | | |
| Cadnano | Douglas et al., 2009a | https://cadnano.org/ |
| CanDo | Kim et al., 2012 | https://cando-dna-origami.org/ |
| SNUPI | Lee et al., 2021 | https://github.com/SSDL-SNU/SNUPI |
| EMAN2 | Tang et al., 2007 | https://blake.bcm.edu/emanwiki/EMAN2 |
| Relion | Scheres, 2012 | https://github.com/3dem/relion.git |
| IMOD | Kremer et al., 1996 | https://bio3d.colorado.edu/imod/ |

## RESOURCE AVAILABILITY

### Lead contact

Further information and requests for resources and reagents should be directed to Yimo Han (yimo.han@rice.edu).

### Materials availability

Materials generated in this study are available from the lead contact upon request.

### Data and code availability

All data reported in the paper are available from the lead contact upon request. This paper does not report original code.

## METHOD DETAILS

### Synthesis of DNA origami

The DNA origami flakes are synthesized using a combination of a long single stranded DNA scaffold with about 250 staple strands to define a cross-tile shape of the 2D DNA flake (Liu et al., 2011). In order to prevent aggregation due to blunt-end stacking at high concentration, the DNA flake was protected by poly-T sticky ends at the extruding edges on all 4 arms. The synthesis details are shown as follows: the long single-stranded scaffold DNA (M13MP18), was mixed with the short staple strands in 1X TAE/$Mg^{2+}$ buffer (40 mM Tris•HCl, 20 mM acetic acid, 2.5 mM EDTA, 12.5 mM magnesium acetate, pH 8.0). The mixture was annealed at 70°C for 20 minutes and cooled to 20°C at a rate of -7°C/h in a thermocycling incubator. The final concentration of the scaffold DNA was 10 nM while that of the staple strands was 80 nM. After synthesis, the excess staple DNA strands were removed by filtering the resulting solution in a 100K Millipore Amicon Ultra 0.5 mL centrifugal filter. The yield was 42% according to UV-Vis measurement. The final product was characterized by air mode AFM (Figure S1).

### Cryo-sample preparation

The 2D DNA monomers were concentrated to 18 nM by multi-cycle centrifuge using 100K Millipore Amicon filters. DNA origami dimers were concentrated to 7 nM. Trimers were concentrated to 1 nM. 4 μL of the DNA origami solution was deposited on Quantifoil cryo-EM grid. We used gold grid with holey carbon support (Quantifoil Au R1.2/1.3, 300 mesh). The wait time is 0.5 minute before the blotting step in Vitrobot. The blotting time ranges from 3 seconds to 5 seconds.

### Cryo-EM

CryoEM images were collected on a 300 kV Cs-corrected Titan Krios using a K2 Summit detector (with GIF Bio-Quantum Energy Filters, Gatan). We collected the raw movies in K2 super-resolution mode at 105,000 x magnification in EFTEM mode, spot size 6, C2 aperture 70 μm. The total exposure time was set to 5.6 s with a 0.175 s frame time to generate 32-frame gain normalized mrc stacks with a nominated pixel size 0.557 Å. The total dose for a stack is 50 $e^-/Å^2$.

### Computational predictions

We used CanDo (Castro et al., 2011; Kim et al., 2012) and SNUPI (Lee et al., 2021) modeling methods to predict the structure and flexibility of the cross-tile DNA origami. By referring to the method described in the supplementary information of work by Wenyan Liu et al.[1], we plotted the origami design in caDNAno (Douglas et al., 2009b) and input it into the CanDo website, as well as the SNUPI software. The coordinates and RMSF of nucleotides were then calculated using CanDo and SNUPI methods, indicating the structure and flexibility of the cross-tile DNA origami. The computational results show great consistency with our experimental observation by cryo-EM.

### Sample preparation for trimers

First, we positively stained DNA trimers using uranyl acetate. 1 μL of the 1.65 nM DNA flake solution was mixed with 2 μL of 1% uranyl acetate solution (in 1X TAE/ $Mg^{2+}$ buffer, freshly filtered) for 3 minutes, then deposited on the graphene cryo-EM grid (Han et al., 2019) for 1 minute before fast freezing using Vitrobot. The monolayer graphene grids were made through a wet transfer process, followed by UV ozone treatment to reduce the hydrophobicity of the graphene and encourage sample adsorption. We allowed the sample to sit on the functionalized graphene for 60 seconds for better surface adsorption. Afterward, we performed the same blotting process using two filter papers to reduce the sample to a thin water layer before vitrification.